J|A|C|S
ARTICLES
Published on Web 12/09/2005

Dynamics of the Degenerate Rearrangement of Bicyclo[3.1.0]hex-2-ene

Charles Doubleday,*,§ Christopher P. Suhrada,‡ and K. N. Houk*,‡

Contribution from the Department of Chemistry, Columbia University, New York, New York 10027, and Department of Chemistry and Biochemistry, University of California, Los Angeles, California 90095

Received February 3, 2005; E-mail: ced3@columbia.edu; houk@chem.ucla.edu

Abstract: Quasiclassical direct dynamics simulations are applied to a 4-fold degenerate rearrangement which yields a nonstatistical product distribution. The simulated product ratio agrees with experiment and is found to be entirely dynamically determined. Trajectory lifetimes are on the order of a low-frequency vibrational period. The interaction of reaction momentum with the geometric features of the potential surface produces selectivity despite a common energy barrier. A geometric model is described for qualitatively estimating much of the dynamically determined product ratio independently of trajectory calculations. The characteristics of this reaction are expected also to apply to others involving modestly stabilized diradical intermediates.

The rates and products of chemical reactions can usually be determined from the energies of transition states, the bottlenecks separating reactants from products. Statistical theories such as the RRKM method and Eyring transition state theory (TST)[1] describe the rates of passage over a potential energy surface in terms of the relative free energies of minima and saddle points, without regard for detailed dynamics elsewhere on the surface.

Several reactions have been investigated where dynamic effects cause behavior that differs from what is predicted by transition state theory.[2−5] In such cases, various minima may be avoided by molecules with sufficient momentum,[6−8] a lowest-energy pathway may be bifurcated by a post-transition-state valley-ridge inflection point,[9,10] and intermediates which do not reach an equilibrium ensemble state may form products in a manner inconsistent with statistical predictions.[11−15]

Some of these examples, especially diradical-mediated rearrangements from the latter category, approach the extreme case where the utter flatness of the potential surface precludes the definite assignment of distinct minima, saddle points, and lowest-energy pathways on the way from a reactant to several products. This type of reaction, involving what has been variously termed a *twixtyl*,[16] *continuous diradical transition state*,[17] or *caldera*,[18] is exemplified in the degenerate rearrangement of bicyclo[3.1.0]hex-2-ene (**1**). A quantitative dynamical treatment of this reaction is described here.

Scheme 1 lays out the degenerate rearrangement of bicyclo-[3.1.0]hex-2-ene labeled with deuterium in the 4-*exo* position (4*x*-**1**). This rearrangement is an example of what Doering has called a "not obviously concerted" reaction:[18] it is not stereospecific, nor does it show the complete stereorandomness expected where equivalent products are formed by degenerate pathways from a single diradical intermediate. The reaction is formally a scission and subsequent re-formation of the endocyclic bond. Upon bond cleavage, a new bond may form in the same position as the old one (a 1,1 shift) or in the equivalent location at the distal end of the allyl unit (1,3). Stereochemical alternatives are *retention* or *inversion* at the original stereocenters and *suprafacial* or *antarafacial* allylic participation. The requirement that the product be a *cis*-fused bi-cycle limits the stereochemical possibilities to 1*r*,1*r* (no reaction), 1*r*,3*s*, 1*i*,1*i*, and 1*i*,3*a*, hereafter abbreviated *rr*, *rs*, *ii*, *ia*. Reactants and products formed on this 4-fold degenerate surface have been distinguished on

§ Columbia University.
‡ University of California, Los Angeles.

(1) Steinfeld, J. I.; Francisco, J. S.; Hase, W. L. *Chemical Kinetics and Dynamics*, 2nd ed.; Prentice Hall: Upper Saddle River, NJ, 1998.
(2) Carpenter, B. K. In *Reactive Intermediate Chemistry*; Moss, R. A., Platz, M. S., Jones, M., Jr., Eds.; Wiley: Hoboken, NJ, 2004; pp 925−960.
(3) Carpenter, B. K. *Acc. Chem. Res.* **1992**, *25*, 520.
(4) Carpenter, B. K. *Angew. Chem., Int. Ed.* **1998**, *37*, 3340.
(5) (a) Cho, Y. J.; Vande Linde, S. R.; Zhu, L.; Hase, W. L. *J. Chem. Phys.* **1992**, *96*, 8275. (b) Hase, W. L. *Science* **1994**, *266*, 998. (c) Sun, L.; Hase, W. L.; Song, K. *J. Am. Chem. Soc.* **2001**, *123*, 5753.
(6) Sun, L.; Song, K.; Hase, W. L. *Science* **2002**, *296*, 875.
(7) Debbert, S. L.; Carpenter, B. K.; Hrovat, D. A.; Borden, W. T. *J. Am. Chem. Soc.* **2002**, *124*, 7896.
(8) Ammal, S. C.; Yamataka, H.; Aida, M.; Dupuis, M. *Science* **2003**, *299*, 1555.
(9) (a) Yamataka, H.; Aida, M.; Dupuis, M. *Chem. Phys. Lett.* **2002**, *353*, 310. (b) Yamataka, H.; Aida, M.; Dupuis, M. *J. Phys. Org. Chem.* **2003**, *16*, 475.
(10) (a) Singleton, D. A.; Hang, C.; Syzmanski, M. J.; Greenwald, E. *J. Am. Chem. Soc.* **2003**, *125*, 1176. (b) Bekele, T.; Christian, C. F.; Lipton, M. A.; Singleton, D. A. *J. Am. Chem. Soc.* **2005**, *127*, 9216.
(11) (a) Carpenter, B. K. *J. Am. Chem. Soc.* **1995**, *117*, 6336. (b) Carpenter, B. K. *J. Am. Chem. Soc.* **1996**, *118*, 10329.
(12) (a) Doubleday, C., Jr.; Bolton, K.; Hase, W. L. *J. Am. Chem. Soc.* **1997**, *119*, 5251. (b) Hrovat, D. A.; Fang, S.; Borden, W. T.; Carpenter, B. K. *J. Am. Chem. Soc.* **1997**, *119*, 5253. (c) Doubleday, C.; Bolton, K.; Hase, W. L. *J. Phys. Chem. A* **1998**, *102*, 3648.
(13) (a) Doubleday, C. *J. Phys. Chem. A* **2001**, *105*, 6333. (b) Doubleday, C.; Li, G.; Hase, W. L. *Phys. Chem. Chem. Phys.* **2002**, *4*, 304.
(14) Reyes, M. B.; Lobkovsky, E. B.; Carpenter, B. K. *J. Am. Chem. Soc.* **2002**, *124*, 641.
(15) Mann, D. J.; Hase, W. L. *J. Am. Chem. Soc.* **2002**, *124*, 3208.
(16) Hoffmann, R.; Swaminathan, S.; Odell, B. G.; Gleiter, R. *J. Am. Chem. Soc.* **1970**, *92*, 7091.
(17) Doering, W. v. E.; Sachdev, K. *J. Am. Chem. Soc.* **1974**, *96*, 1168.
(18) Doering, W. v. E.; Cheng, X.; Lee, K.; Lin, Z. *J. Am. Chem. Soc.* **2002**, *124*, 11642.

 10.1021/ja050722w CCC: $33.50

Scheme 1

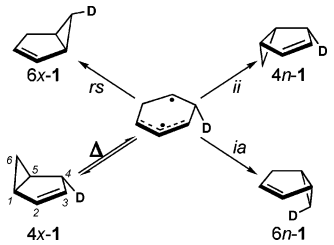

Table 1. Relative Rates (%) Measured for Formation of *rs*, *ii*, and *ia* Products from Three Derivatives of **1** in the Gas Phase

educt	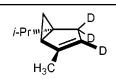		
rs	49	51	48
ii	32	38	36
ia	19	11	16
reference	(19b)	(20)	(21)

the basis of deuterium labeling and optical activity, first for the natural product derivative thujene[19] and later for bicyclo[3.1.0]-hex-2-ene itself.[20,21] These studies have revealed relative rates for *rs*, *ii*, and *ia* processes in a ratio of about 3:2:1 in the gas phase (Table 1). Here we focus our analysis on the most recent experimental study, in which Baldwin and Keliher[21] measured k_{rs}:k_{ii}:k_{ia} = 48:36:16 (Scheme 1) and found that the three pathways have identical activation parameters within experimental error.

Our examination of the shape of the potential energy surface (PES) for the rearrangement of **1** indicated a case of degenerate products formed by equi-energetic but geometrically nonequivalent pathways.[22] The points **TS**, ***C*$_S$**, and ***C*$_{2v}$** (Figure 1) are so nearly isoenergetic that they effectively constitute a single potential energy plateau,[23] which, for the sake of simplicity, we will refer to in this manuscript as "the caldera". Figure 2 shows two views of the PES; the caldera is the extend region (yellow) bounded by and having energy essentially identical to the four structures **TS**. Reaction pathways across this isoenergetic region are not equivalent because, although the PES has 4-fold symmetry, only one of the four isomers is the reactant. Now, direct dynamics trajectory simulations confirm how this diradical species with no minimum on the potential energy surface and a lifetime on the order of low-frequency molecular vibrations leads to the disparate product distribution observed experimentally.

Computational Details

Trajectory simulations were run on a semiempirical surface, AM1-SRP (AM1 with specific reaction parameters), created by modifying an AM1 potential to fit our previously published CASPT2(4,4)/6-31G*//CASSCF(4,4)/6-31G* results.[22] To construct the AM1-SRP Hamiltonian, AM1 resonance integrals for C_1-C_5 and C_3-C_5 interactions were modified[12c] according to

$$H_{ij}^{ab} = \chi_{ij}^{ab}(R_{ij})H_{ij}^{0,ab} \tag{1a}$$

$$\chi_{ij}^{ab}(R_{ij}) = \chi_{ij,\mathrm{small}}^{ab} + \frac{1}{2}(\chi_{ij,\mathrm{large}}^{ab} - \chi_{ij,\mathrm{small}}^{ab})[1 + \tanh(f_{ij}(R_{ij} - R_{ij}^{0}))] \tag{1b}$$

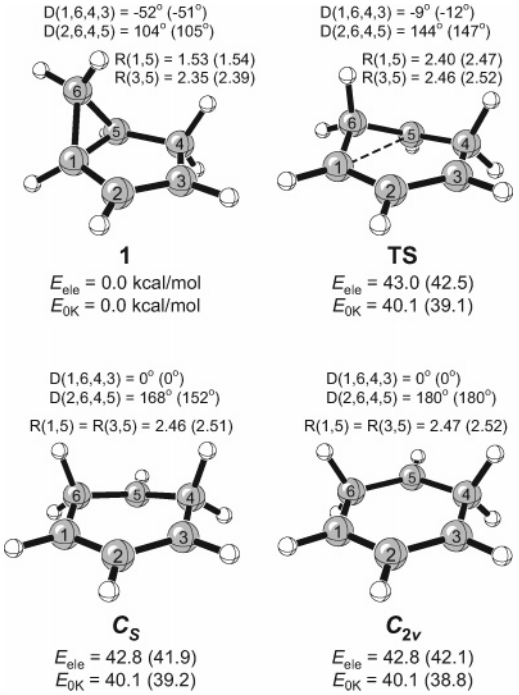

Figure 1. Stationary points on the AM1-SRP surface. Bond lengths are in angstroms, energies (relative to **1**) are in kcal/mol. Ab initio values are listed in parentheses. Ab initio geometries were optimized with CASSCF-(4,4)/6-31G*, and their energies were computed at the CASPT2(4,4)/6-31G* level.[22] E_{ele} excludes the zero-point vibrational energy correction; E_{0K} includes it.

where R_{ij} is the distance between atoms i and j (= 1,3 or 1,5); $H_{ij}^{0,ab}$ is the standard AM1 resonance integral, and *ab* labels the overlap type (ss, sp, pp). The scaling factor $\chi_{ij}^{ab}(R_{ij})$ switches from $\chi_{ij,\mathrm{small}}^{ab}$ at small values of R_{ij} to $\chi_{ij,\mathrm{large}}^{ab}$ at large R_{ij}; $R^0{}_{ij}$ and f_{ij} are constants for a given i,j.

AM1-SRP has 32 parameters that differ from the AM1 parameter set. Seventeen of these are revised AM1 parameters for C and H, and fifteen are associated with eq 1. The fit was carried out by minimizing the weighted sum of squared differences between ab initio and AM1-SRP energies and geometries using a genetic algorithms package.[24] Figure 1 shows AM1-SRP stationary points and relative energies, with the corresponding ab initio values[22] in parentheses. Tables of AM1-SRP parameters, internal coordinates, energies, and frequencies of AM1-SRP stationary points are included in the Supporting Information.

Figure 2 shows a projection of the AM1-SRP surface onto the 2D space defined by dihedral angles *D*(1,6,4,3) and *D*(2,6,4,5). This surface is very similar to the previously published CASSCF surface,[22] except that the AM1-SRP caldera in Figure 2, based on CASPT2, is even flatter—structures **TS**, ***C*$_S$**, and ***C*$_{2v}$** all lie within a range of 0.2 kcal/mol.

In this study, we compute the product ratio derived from 4*x*-**1** as the reactant. This is done by simulating the dynamics of Scheme 1 by a quasiclassical trajectory method, focusing on the caldera region of the PES. The TS normal mode sampling procedure[12c] is used to generate a set "TS_0" of initial coordinates and momenta that approximates a

(19) (a) Doering, W. v. E.; Lambert, J. B. *Tetrahedron* **1963**, *19*, 1989. (b) Doering, W. v. E.; Schmidt, E. K. G. *Tetrahedron* **1971**, *27*, 2005.
(20) Cooke, R. S.; Andrews, U. H. *J. Am. Chem. Soc.* **1974**, *96*, 2974.
(21) Baldwin, J. E.; Keliher, E. J. *J. Am. Chem. Soc.* **2002**, *124*, 380.
(22) Suhrada, C. P.; Houk, K. N. *J. Am. Chem. Soc.* **2002**, *124*, 8796.
(23) ***C*$_S$** and ***C*$_{2v}$** are technically stationary points on the UB3LYP and CASSCF electronic energy surfaces, but the energy difference between them and **TS** is practically negligible, and it diminishes further at the CASPT2 level and with the inclusion of zero-point and thermal corrections (see ref 22). They serve here as key reference points for the AM1-SRP reparametrization, but trajectory simulations show that they have no more dynamical significance than any other part of the caldera.
(24) Carroll, D. L. *AIAA J.* **1996**, *34*, 338; program obtained from http://www.staff.uiuc.edu/~carroll/ga.html.

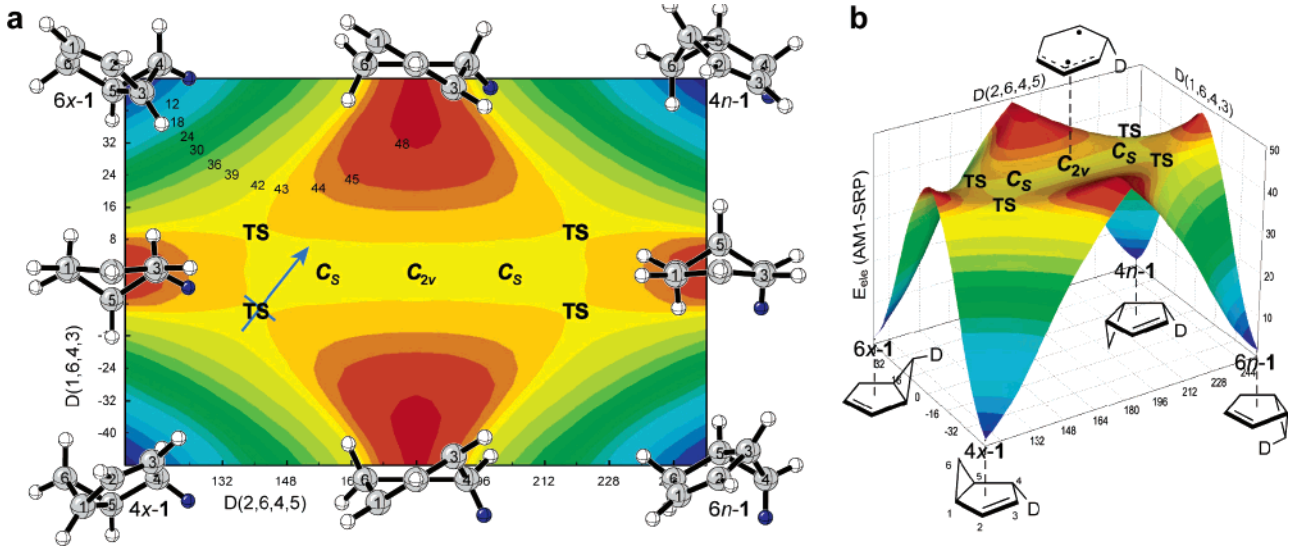

Figure 2. Two views of the AM1-SRP potential energy surface. Contour interval is 3 kcal/mol, with additional contours added at 43 and 44 kcal/mol. All points in the caldera region, bounded by the four points **TS**, lie within an energy range of only 0.2 kcal/mol. On the 2D plot, the arrow points along the transition vector (imaginary frequency eigenvector at the saddle point), and dark blue shading denotes the deuterium label position in the accompanying structures.

Table 2. Percent Yields[a] Derived from Trajectories at 498 and 528 K[b]

	498 K	528 K	expt
rs	47.0 ± 1.7	47.2 ± 1.7	48
ii	37.6 ± 1.7	37.8 ± 1.7	36
ia	15.4 ± 1.3	15.0 ± 1.3	16

[a] Uncertainties are at the 95% confidence level. [b] Of ca. 4000 trajectories run at each temperature, 81% are reactive.

quantum mechanical Boltzmann distribution on the TS dividing surface separating 4*x*-**1** from the caldera. This method is based on the assumption that TST accounts for the forward flux of trajectories moving from the reactant through the TS dividing surface onto the caldera, and that the TS dividing surface intersects the saddle point. After initial conditions are selected, Hamilton's equations of motion are integrated on the AM1-SRP surface with a step size of 0.25 fs. Each trajectory is integrated forward and backward in time from its initial point until an isomer of **1** is formed in each direction. A trajectory is counted as reactive if either the forward-time or backward-time segment leads to 4*x*-**1** and the other segment leads to one of the other three isomers. The calculations are carried out with Venus-Mopac,[25] a combination of the dynamics program Venus 96[26] with the Mopac 7 semiempirical electronic structure package,[27] modified by incorporation of AM1-SRP.

Results and Discussion

Table 2 gives product distributions from simulations at the highest and lowest experimental temperatures reported by Baldwin.[21] Within the uncertainties of theory and experiment, the two agree remarkably. Consistent with experimental results, the simulated product distribution is independent of temperature.

Watching trajectories move over the surface helps one to understand the product ratios. Figure 3 shows snapshots at 30 fs intervals of the 3240 reactive trajectories at 498 K, synchronized to the initial TS point as the zero of time. Additional features appear in the animations at 2.5 fs per frame (see Supporting Information). At the saddle point, TS_0 occupies a band perpendicular to the transition vector (the imaginary frequency eigenvector, arrow in Figure 2a). On this flat surface, the thermal population spans the entire space between the hills on either side of the saddle point. As trajectories evolve from TS_0, their mean and most probable initial direction is along the transition vector, but with a large variance, and they soon become dispersed over the surface. Trajectory points are colored according to the product they eventually form.

Nearly all trajectories make just a single pass through the caldera and leave through the wide exit channels in one continuous motion. In the following paragraphs, we examine how the product distribution results from the shape of the potential energy surface, its interaction with momentum in the reaction coordinate, and its manifestations in the microscopic time course of the reaction.

Trajectories traverse the caldera much faster than energy can be redistributed to other vibrational modes, and momentum is roughly conserved in the 2D space defined in Figure 2.[28] From the entrance channel, the transition vector directs most trajectories toward the high-energy region separating the *rs* and *ii* exit channels. Necessarily, about as many trajectories have momentum leftward of the transition vector as have momentum to the right of it. Those that move to the left are quickly, irreversibly trapped in the nearby *rs* exit channel. Those tending to the right have much farther to travel before reaching the *ii* and *ia* products, but they do so almost exclusively; the extent to which the fate of a molecule can be decided almost immediately after it enters the caldera is reflected in the fact

(25) Peslherbe, G. H.; Bolton, K.; Doubleday, C.; Hase, W. L. *VENUS-MOPAC*, A General Chemical Dynamics Computer Program, Including Qm and QM+MM Semiempirical Direct Dynamics. To be released.
(26) Hase, W. L.; Duchovic, R. J.; Hu, X.; Komornicki, A.; Lim, K.; Lu, D.-H.; Peslherbe, G. H.; Swamy, K. N.; Vande Linde, S. R.; Wang, H.; Wolfe, R. J. *VENUS 96*, a General Chemical Dynamics Computer Program. *QCPE* **1996**, 671.
(27) Stewart, J. J. P. *MOPAC 7*, A General Molecular Orbital Package. *QCPE* **1993**, 455; *J. Comput. Chem.* **1989**, *10*, 209.
(28) The two dihedral angles, *D*(1,6,4,3) and *D*(2,6,4,5), represent a convenient but nonrigorous coordinate system within which to map the PES and to present our analysis; they are not strictly orthogonal, and they are not weighted in terms of atomic masses. These coordinates are in no way inherent to the trajectory simulations themselves, but they are useful geometric parameters for monitoring the course of those trajectories. The use of these internal coordinates to describe trajectory momenta is grossly approximate, but qualitatively instructive.

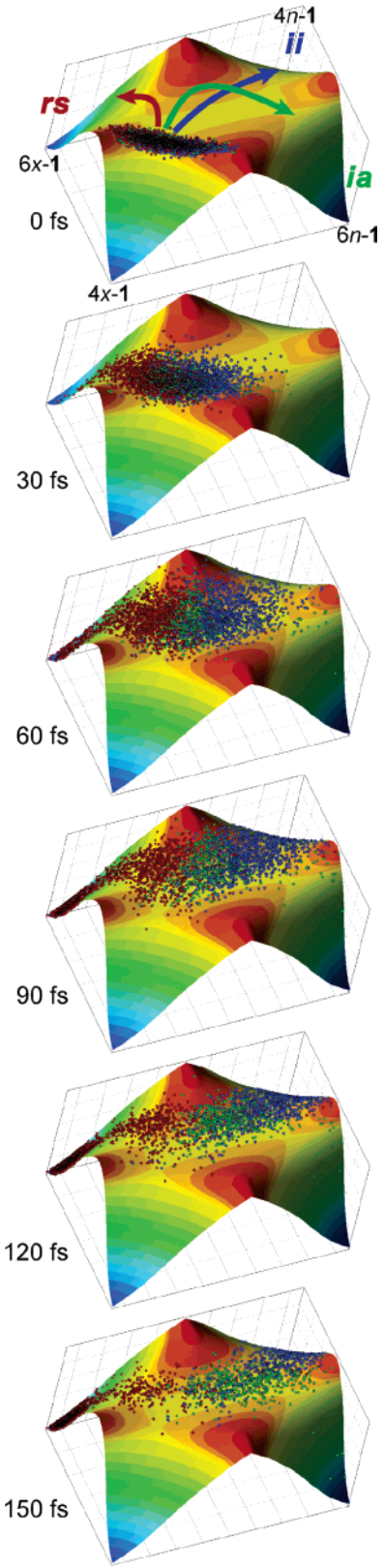

Figure 3. Snapshots at 30 fs intervals of reactive trajectories at 498 K. Time zero is the TS point at which each trajectory is initialized. Arrows in the 0 fs frame show approximate mean paths of trajectories leading to a given product: *rs* (red), *ii* (blue), and *ia* (green). Trajectory points are colored according to the product each ultimately forms. Axes are as labeled in Figure 2b.

that 97% of those molecules which reach $D(2,6,4,5) \geq 180°$ go on to form *ii* and *ia* products.

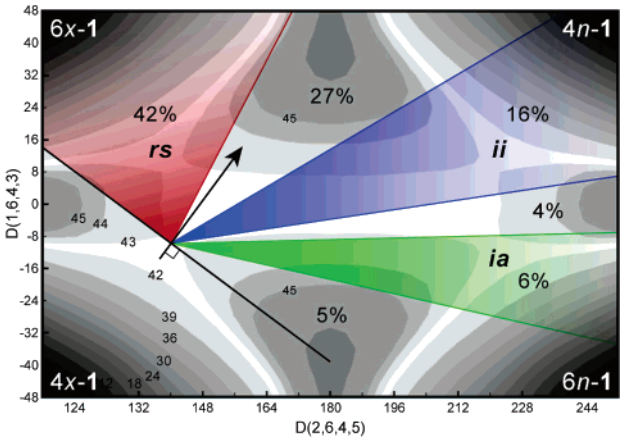

Figure 4. Estimated reactive angular ranges for straight-line trajectories across the caldera. Contours are labeled in kcal/mol; arrow is the transition vector ($\theta = 0$). Trajectories move radially out from the caldera entrance (structure 4*x*-**TS**) over a 180° arc. The arc is divided into six angular ranges, weighted according to (1/2)cos θ. Colored segments represent unobstructed paths to products: *rs* (red, 42%), *ii* (blue, 16%), and *ia* (green, 6%). Nonshaded portions (36% total) do not lead directly to any exit channel and, therefore, are not assigned a priori to any particular product.

In contrast, the productivity of initial momentum in the positive $D(1,6,4,3)$ direction is diminished because the location of exit channels is not ideal. Fully 95% of all trajectories are carried by their initial momentum to values of $D(1,6,4,3) > +12°$, the value of $D(1,6,4,3)$ in the *rs* and *ii* exits, but only 85% actually form *rs* and *ii* products. The remaining 10% reverse direction and find the *ia* product instead because they reach $D(1,6,4,3) > +12°$ not in the vicinity of the *rs* or *ii* exits but in the high-energy region in between.

The tendency for momentum to be conserved or redirected can be understood in terms of the PES shape. The caldera region is elongated, with broad shallow exit channels at the corners and upward slopes along the north and south walls. Within this region, the flatness of the PES means that most trajectories follow approximately straight paths. Consequently, the behavior of many trajectories can be crudely but instructively modeled by considering an angular distribution, emanating from the caldera entrance, centered about the transition vector.

The red, blue, and green shaded segments in Figure 4 represent unobstructed paths from the caldera entrance to each of the three exit channels.[29] TS_0 is approximated in the figure as a single point rather than an ensemble distributed along the dividing surface. Defining θ as a given trajectory's deviation from the transition vector, we assume a cos θ distribution of the initial directions taken by trajectories as they emerge from 4*x*-**TS** onto the caldera.[30] This distribution has a reasonable shape: largest at the transition vector, and dropping to zero at $\pm 90°$. With these assumptions, we estimate the fractional product yield from each colored segment with angular range from θ_1 to θ_2 as $(1/2)\int \cos\theta d\theta$.

According to this approximation, 42% of trajectories will proceed relatively unhindered to *rs*, 16% to *ii*, and only 6% to *ia*. The remaining fractions (36% total) do not lead directly to

(29) We arbitrarily define 45 kcal/mol—TS energy plus 2*RT* at 513 K—as the limit for what is considered a potential energy "obstruction".
(30) The choice of cos θ is a two-dimensional adaptation of Carpenter's multidimensional vector model for a nonstatistical product ratio. This model gives good to excellent agreement with experiment in the several cases to which it has been applied. See refs 2 and 4, and: Peterson, T. H.; Carpenter, B. K. *J. Am. Chem. Soc.* **1992**, *114*, 766.

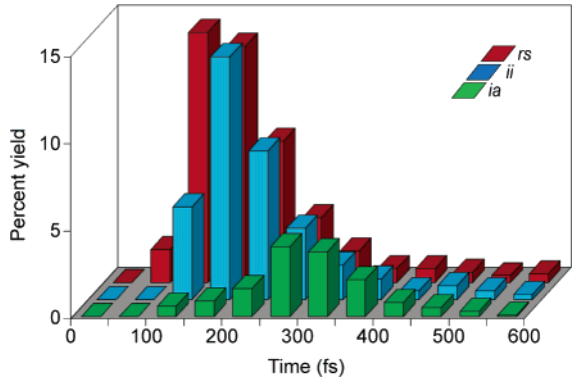

Figure 5. Percent yields at 528 K, formed within 50 fs intervals, derived from trajectories that lead from reactant at time zero to *rs* (red), *ii* (blue), and *ia* (green). In this 600 fs window, the total yield of all products is 98%. The infinite time sum of yields for each product is given in Table 2.

the exit channels, and their fate is less predictable. The most significant of these is the 27% portion directly about the transition vector which is headed for the high-energy region between 6*x*-**1** and 4*n*-**1**. How such an upslope will alter the momentum of trajectories and to deflect them in new directions is difficult to predict quantitatively. The simulations show that the results are small-angle deflections into *ii* and large-angle deflections into *ia*. We note that, even among such redirected trajectories, there is little randomization—a reasonable comparison would be to bank shots on a pool table. It appears appropriate based on the simulations to conclude that the product distribution here is highly determined by the vibrational momentum of the reacting molecules and how that momentum is filtered and funneled by the features of the PES.

Figure 5 shows simulated product yields, within successive 50 fs intervals. The yields are computed over trajectory lifetimes defined as the sum of the forward- and backward-time durations, that is, from 4*x*-**1** through the TS to the product. Fully 95% of trajectories traverse the caldera in less than 400 fs—approximately the period of a low-frequency molecular vibration. Additionally, an important feature of this and other reactions involving nonstatistical dynamics[4,13] is that the product ratio is time-dependent on the microscopic level.[31] Below 150 fs, *rs* is almost the only product formed; by 200 fs, *ii* has caught up, and the two then evolve in parallel. The *ia* yield accumulates much more slowly. These different time frames relate directly to the geometric nonequivalence of the *rs*, *ii*, and *ia* pathways.

The *rs* major product is formed primarily by direct trajectories: 96% never leave $D(2,6,4,5) < 180°$. The nearness of the *rs* exit channel to the caldera entrance allows it to trap a large fraction of the angular distribution as described above. This same conformational propinquity, identified qualitatively by Doering in the original studies,[19] along with the fact that there is minimal deflection along the way, accounts for the speed with which *rs* is populated relative to the other products.

The *ii* product occupies the second-largest weighted angular range as viewed from the entrance channel across the caldera. In addition, the *ii* exit channel is in a position to capture most of those trajectories which are shallowly deflected by the top hill. Either way, most *ii* trajectories proceed to that product with little extraneous motion. It is the relatively large conformational distance separating *ii* from the reactant which causes the formation of *ii* to lag substantially behind *rs* in time.

The minor product finds itself at a distinct disadvantage in terms of its prospects for formation by direct motion from the entrance channel due to its small angular range, which lies at a high angle from the transition vector. For this reason, only a very small fraction of *ia* trajectories proceed directly from the caldera entrance to their exit. Although they both enter and leave the caldera at $D(1,6,4,3) < 0°$, some 92% of *ia* trajectories sample the conformational space at $D(1,6,4,3) > 0°$ at some time in between. More than two-thirds (68%) actually reach $D(1,6,4,3) > +12°$ — the value of $D(1,6,4,3)$ in the *rs* and *ii* exit transition states—before reversing direction and attaining the *ia* exit channel. The fact that so many *ia* trajectories are thus reflected, in contrast to the relatively direct routes to *rs* and *ii*, means that they must cover more ground on the way to their destination and necessarily take more time to reach it.

Conclusion

Trajectory simulations show how dynamics differentiate geometrically between equi-energetic pathways from a single reactant to three identical products. It appears that many trajectories can be understood in terms of straight paths from the caldera entrance to the various exit channels. To the extent that these straight-line trajectories are in the majority, the product distribution can be qualitatively related to the geometric disposition of products relative to the transition vector. However, we also find a substantial fraction of trajectories which, delivered by their initial momentum into high-energy PES regions, are deflected from their original course and into the exit channels in a less predictable way. The diradical intermediate, if it may even be considered as such, has a lifetime only long enough to accomplish a continuous structural change from reactant to product, and the different conformational demands for formation of the various products are manifest in the different time durations required to reach them.

While quantitative conclusions made here are strictly applicable to bicyclo[3.1.0]hex-2-ene only, the features of its potential energy profile—no significant minima on a broad, flat intermediate surface—have also been found for other reactions, including vinylcyclopropane−cyclopentene,[13,32] vinylcyclobutane−cyclohexene,[33] and bicyclo[3.2.0]heptene−norbornene[11] rearrangements, as well as the stereomutation of cyclopropane.[12] In the absence of significant stabilization of the diradical by extended conjugation on both radical centers, the PES and dynamical features described here are likely to be of general significance.

Acknowledgment. The authors gratefully acknowledge financial support from the National Science Foundation, as well as a grant of computing resources from the National Center for Supercomputing Applications (project *ooe*).

Supporting Information Available: AM1-SRP definition and parameters; AM1-SRP stationary point energies, geometries, and frequencies (PDF). This material is available free of charge via the Internet at http://pubs.acs.org. Trajectory animation is available online at http://www.columbia.edu/∼ced3.

JA050722W

(31) Such time dependence would not, of course, be observed experimentally since the reactions of individual molecules are distributed in time by many orders of magnitude compared to the duration of reaction of any single molecule.

(32) (a) Houk, K. N.; Nendel, M.; Wiest, O.; Storer, J. W. *J. Am. Chem. Soc.* **1997**, *119*, 10545. (b) Doubleday, C.; Nendel, M.; Houk, K. N.; Thweatt, D.; Page, M. *J. Am. Chem. Soc.* **1999**, *121*, 4720.
(33) Northrop, B. H.; Houk, K. N. *J. Org. Chem.* In press.